Journal of Power Sources 231 (2013) 113–121

Contents lists available at SciVerse ScienceDirect

Journal of Power Sources

journal homepage: www.elsevier.com/locate/jpowsour

High stability of low Pt loading high surface area electrocatalysts supported on functionalized carbon nanotubes

Daniela Z. Mezalira, Michael Bron*

Technische Chemie I, Institut für Chemie, Naturwissenschaftliche Fakultät II, Martin-Luther-Universität Halle-Wittenberg, von-Danckelmann-Platz 4, 06120 Halle, Germany

HIGHLIGHTS

- ► Nano-size Pt particles on functionalized CNTs are synthesized by the polyol method.
- ► Catalyst resistance to degradation by testing ECSA loss/ORR activity in stress test.
- ► ECSA loss is comparably small and virtually independent of CNTs functionalization.
- ► Initial strong changes in ECSA are attributed to structural changes in the catalyst.

ARTICLE INFO

Article history:
Received 19 September 2012
Received in revised form
3 December 2012
Accepted 6 December 2012
Available online 20 December 2012

Keywords:
Functionalized carbon nanotubes
Pt nanoparticles
High surface area electrocatalysts
Oxygen reduction reaction
Catalyst stability

ABSTRACT

Functionalized (N, O) carbon nanotubes supported Pt electrocatalysts with high surface area and small average particle diameter (2 nm) are synthesized by the polyol method using microwave irradiation. Physical and electrochemical methods are used to characterize the surface and the structure of the catalysts and supports. The stability of the catalysts is evaluated through an accelerated stress test by fast potential cycling monitoring changes in electrochemical behavior with cyclic voltammetry and polarization curves. Characterization indicates that the Pt particle size is comparable for all samples and is about 2 nm with a Pt loading depending on the carbon nanotubes employed in synthesis. The accelerated stress test demonstrates that the electrochemical surface areas (ECSAs) are relatively stable and only a small and non-linear decay is observed, which is much lower than with carbon black-supported samples. Strikingly, the ECSA loss is virtually independent of the composition/functionalisation of the CNTs. Initial stronger changes in ECSA are tentatively attributed to initial structural changes in the catalyst, which are more pronounced for CNT and oxygen-functionalized CNT (OCNT) supported samples. Concurrently, the surface specific activity initially changes strongly in the latter samples, while it does not for the nitrogen-functionalized CNT (NCNT) supported catalysts.

1. Introduction

Fuel cells are devices which directly convert chemical into electrical energy avoiding the thermo-mechanical energy conversion of e.g. combustion engines and may thus achieve efficiencies much higher than the Carnot limit. Furthermore, when run on hydrogen, fuel cells provide clean energy production where the only by-product formed is water ($H_2 + ½O_2 \rightarrow H_2O$). In such a device hydrogen is oxidized at the anode ($H_2 \rightarrow 2H^+ + 2e^-$) while oxygen is reduced at the cathode ($½O_2 + 2H^+ + 2e^- \rightarrow H_2O$). Both electrodes are separated by a typically solid electrolyte, e.g. a proton conducting membrane, while the external electrical circuit allows transport of electrons [1]. Platinum (Pt) is widely recognized as the most active metal for the anodic oxidation of H_2 as well as for the cathodic reduction of O_2 [2–4]. Due to the high cost of the metal, it should be well dispersed onto a high surface area support to increase Pt surface area while simultaneously using lower amounts of Pt. In addition, besides dispersing the active phase, the support provides a porous structure, prevents sintering, improves mechanical strength and may assist in catalysis [5]. However, currently used carbon materials for the preparation of electrocatalysts are carbon black-type materials, which are well known to be electrochemically unstable and to corrode under the conditions found in PEM fuel cells leading to Pt particle dissolution, agglomeration or detachment [6–12]. No surprise there are ongoing research activities looking for more stable support materials. Presenting distinct electronic and structural properties, nanostructured materials such as carbon nanotubes (CNTs) offer many

* Corresponding author. Tel.: +49 345 5525900; fax: +49 345 5527163.
E-mail address: michael.bron@chemie.uni-halle.de (M. Bron).

0378-7753/$ – see front matter © 2012 Elsevier B.V. All rights reserved.
http://dx.doi.org/10.1016/j.jpowsour.2012.12.025

advantages to be used as supports for metal catalysts and have been extensively studied for this application [13,14]. It has been reported that these nanostructured materials exhibit higher electrochemical corrosion resistance and improve the stability of Pt supported catalysts in comparison to conventional carbon black supports [15,16]. However, due to the hydrophobic and inert surface of this material, it is difficult to achieve a favorable interaction and dispersion of metal particles on CNTs. Functionalization of these CNTs to incorporate heteroatoms like N and O into the surface can enhance the affinity between the metal and carbon, favoring the incorporation of metallic nanoparticles and avoiding agglomeration problems [13]. Moreover, the incorporation of nitrogen atoms recently has received considerable attention due to improvement in catalytic activity for the oxygen reduction reaction (ORR) and also the durability of the carbon supports during electrocatalytic processes [17–21].

In the present study we examine the stability of platinum supported on modified CNTs through electrochemical measurements and compare samples with different surface functional groups. The catalysts were prepared using commercial carbon nanotubes, functionalized or not, as well NCNTs grown via chemical vapor deposition (CVD), as support materials. Low loading high specific surface area catalysts were prepared, avoiding extensive agglomeration of particles already during the preparations step and allowing monitoring significant changes in the specific surface area by aging. The corresponding physicochemical properties of these catalysts were studied by transmission electron microscopy, Raman spectroscopy, thermogravimetric analysis, inductively coupled plasma–optical emission spectroscopy, and elemental analysis. The stability of all catalysts was investigated monitoring electrochemical surface area (ECSA) and catalytic activity after every 500 cycles of an accelerated stress test.

2. Experimental methods

2.1. Support preparation

Commercial multi-walled carbon nanotubes (Baytubes® C 150 P) were purchased from Bayer Materials Science.

To activate the CNTs surface an acid treatment (OCNTs) was carried out by refluxing in 5 M HNO_3 at 100 °C for 6 h. Generally, functional groups such as –COOH or –OH are created on the CNTs surface during such oxidation [22,23]. The damage induced into the surface of the CNTs by our treatment is much less severe than by the typically used treatment with concentrated nitric acid. In the latter case, layers of amorphous material form which surround the CNTs, and which do not form with our treatment. These layers might influence the stability behavior of the catalysts and their formation thus should be avoided to be able to doubtlessly monitor the effects induced by functional groups. After treatment, the carbon nanotubes were separated by centrifugation and washed with ultrapure water, until the pH of the wash water was neutral, and dried at 110 °C overnight.

For nitrogen incorporation (NCNTs), 100 mg of OCNTs were heated under ammonia gas (10% in He) at 400 °C for 6 h with a flow rate of 1.5 L h^{-1}, following literature [20,24]. According to the authors, at this temperature, mainly pyridinic and pyrrolic groups are introduced into the CNTs surface.

Carbon nanotubes containing nitrogen ($NCNTs_{-CVD}$) were also synthesized by chemical vapor deposition over silica (SiO_2 – aerosil 380 provided by Evonik) supported iron catalyst. A 20 wt.% Fe catalyst was prepared by a homogeneous deposition precipitation method, as proposed by Van Dommele et al. [25], and then calcined at 500 °C for 3 h. Acetonitrile (CH_3CN, Roth) CVD was performed by placing 0.15 g of Fe/SiO_2 into a quartz boat inside a quartz tube in a horizontal furnace. Before the NCNTs growth, the active metal components were reduced by heating at 650 °C for 1 h in 15% H_2/Ar at a flow rate of 3 L h^{-1}. Then, the argon stream was saturated with acetonitrile at room temperature by flowing through an acetonitrile bubbler, at a flow rate of 6 L h^{-1}, and then fed to furnace. The acetonitrile pyrolysis continued for 2 h at 650 °C followed by cooling the oven to room temperature in argon. The as-synthesized samples were purified by subsequent hydrochloric acid (HCl) and potassium hydroxide (KOH) washes: To remove the metal catalyst particles, the nanotubes were refluxed in 1 M HCl for 1 h and then washed with ultrapure water to remove the residual HCl. Next, the samples were refluxed in 1 M KOH for 1 h to dissolve the support remaining from the growth catalyst and washed with ultrapure water until the pH of the wash water was neutral. The recovered CNTs were dried at 110 °C overnight.

2.2. Deposition of platinum nanoparticles

Platinum catalysts were prepared by the polyol method using microwave irradiation [26,27]. 100 mg of carbon nanotubes (CNTs, OCNTs, NCNTs, or $NCNTs_{-CVD}$) were mixed with 50 mL of ethylene glycol (EG) and the solution was sonicated for 30 min to achieve a homogeneous suspension. Afterward, chloroplatinic acid (H_2PtCl_6, Acros Organics) was added to the suspension to obtain a platinum loading of 10 wt.% and sonicated for additional 30 min. The pH was adjusted to 10 using a solution of 0.05 M KOH in EG to induce small and uniform platinum particle formation [28]. Then, the suspension was placed in a microwave oven (MLS Start) and heated twice at 700 W for 75 s. The fast heating by microwave accelerates the reduction of the metal precursor and the nucleation of the metal clusters [26]. After cooling down to room temperature and stirring overnight, the resulting suspension was centrifuged and the solid retained was thoroughly washed with ultrapure water and centrifuged again. This step was repeated five times. Finally, the remaining solid was dried at 110 °C overnight.

2.3. Physical characterization

A LEO912 OMEGA microscope operating at 120 kV was used for Transmission Electron Microscopy (TEM) and the samples were deposited on 3.05 mm copper grids (300 mesh). The mean particle size and size distribution were evaluated by measuring the diameter of isolated particles in an arbitrary area. Between 400 and 500 particles were considered for each catalyst in order to have an acceptable statistical sample. The diameter of carbon nanotubes prepared by CVD was also determined from micrographs (304 nanotubes were analyzed).

Raman spectra of CNTs were obtained at room temperature with a Renishaw inVia spectrometer equipped with a Leica DM2500 M confocal microscope, using a Cobolt CW DPSS Laser. The Raman scattering was excited using 532 nm as excitation wavelength and detected with a CCD camera. Spectra were recorded in the 100–3200 cm^{-1} Raman shift range. The carbon ordering degree was evaluated by means of the relative intensities of D (ca. 1350 cm^{-1}) and G (ca. 1590 cm^{-1}) bands.

Thermogravimetric analysis (TGA) was carried out with a Netzsch thermobalance (STA449 F1 Jupiter®), in alumina crucibles, to determine the stability of the CNTs. The measurements were performed under 10% O_2/Ar flow of 3 L h^{-1}. The temperature was varied from 35 °C to 1000 °C with a heating rate of 10 °C min^{-1}.

Inductively coupled plasma–optical emission spectroscopy (ICP–OES Horiba Jobin Yvon Ultima 2) was performed to quantify the metal loading in the platinum supported electrocatalysts. The catalysts have been digested in aqua regia under microwave heating with a micro PREP 1500 (MWS Vertriebs-GmbH, Leutkirch,

Germany). Non-dissolved CNTs were separated by centrifugation. After dilution with water their concentrations were determined with ICP–OES. A catalyst of known metal loading (20 wt.% Pt/C, E-TEK) has been treated in the same way to validate the procedure.

Elemental analysis (EA) was carried out to determine the nitrogen content with a Vario EL (CHNS) analyzer.

2.4. Electrochemical measurements

All electrochemical measurements were carried out at room temperature in a single compartment three-electrode cell connected to an Autolab potentiostat system (PGSTAT128N, Metrohm) controlled by NOVA software. A reversible hydrogen electrode (RHE) and Pt wire were used as reference and counter electrode, respectively. For the working electrode a catalyst ink was prepared. The catalyst was dispersed by sonication in 300 μL of isopropanol and 50 μL of Nafion® 117 solution (Aldrich) for 1 h to form a uniform ink. Before each working electrode preparation, the catalyst suspension was again put into the ultrasonic bath for 10 min to homogenize the suspension using the same catalyst ink for at most 2 weeks. A volume of 5 μL of the ink was pipetted and spread onto a polished glassy carbon rod (4 mm diameter, 0.126 cm^2 geometrical surface area) embedded in Teflon and the electrode was dried overnight in an atmosphere saturated with isopropanol. The platinum loading was kept at 21 μg_{Pt} cm^{-2}, calculated based on the real Pt loading determined by ICP–OES (see below). Before each experiment, a drop of electrolyte was dropped onto the tip of the working electrode, and the electrode was left for at least 20 min to fully wet the catalyst coating. Afterward, the Pt catalyst was electrochemically cleaned to remove any adsorbed chemical species by sweeping the potential from the limits of 0.05–1.2 V vs. RHE at a scan rate of 0.1 V s^{-1} for 50 cycles.

Both, underpotential hydrogen deposition (H_{upd}) and CO-stripping were used to determine the electrochemical surface area (ECSA). H_{upd} was carried out in nitrogen saturated acidic media (0.1 M $HClO_4$, Roth) by cycling 3× at a scan rate of 0.1 V s^{-1} between 0.05 V and 1.2 V vs. RHE. The second cycle was used for calculation. For the CO-stripping voltammograms, 0.5 M H_2SO_4 was purged with N_2 for 20 min to remove any dissolved reactive gases from the electrolyte. Afterward, carbon monoxide (CO) gas was purged for 20 min while keeping the electrode at a potential of 0.05 V vs. RHE. Then, the dissolved CO was removed by bubbling nitrogen into the solution for additional 20 min, and the stripping voltammograms were recorded at a scan rate of 0.02 V s^{-1}.

The catalysts resistance to degradation was evaluated by an accelerated stress test applying continuous potential cycling between 0.1 and 1.3 V vs. RHE at a scan rate of 1 V s^{-1} in nitrogen saturated 0.1 M $HClO_4$ solution. Each treatment procedure consisted of 500 cycles and was repeated five times. Between each repetition, the decay processes were evaluated by in situ electrochemical tests, namely cyclic voltammetry (CV) and oxygen reduction reaction (ORR) measurements. The cyclic voltammograms were recorded from 0.05 to 1.2 V vs. RHE at 0.1 V s^{-1} scan rate and the system was thoroughly degassed for 20 min with pure nitrogen prior to analysis. The polarization curves were obtained using a rotating disc electrode (RDE) in the potential range of 0.05–1.05 V vs. RHE at a scan rate of 0.005 V s^{-1} using three different electrode rotation speeds: 400, 900, and 1600 rpm. Pure oxygen was used to purge the solution for 20 min to achieve oxygen-saturated electrolyte solution. As the accelerated stress test was performed in N_2 saturated solution after each ORR measurement the electrolyte was replaced for a fresh 0.1 M $HClO_4$ solution.

The ORR activity and selectivity were evaluated by data analysis using the Koutecky–Levich equation (Equation (1)) [29]:

$$1/j = 1/jk + \left(1/0.62nFc_{O_2}D_{O_2}^{2/3}\nu^{-1/6}\omega^{1/2}\right) \quad (1)$$

where j is the current density (A cm^{-2}), j_k is the kinetic current density (A cm^{-2}), n is the average number of electrons transferred per molecule of O_2, F is Faraday's constant (96,485 C mol^{-1}), c_{O_2} is the concentration of dissolved O_2 in 0.1 M $HClO_4$ at 20 °C (1.38×10^{-6} mol cm^{-3}) [29], D_{O_2} is the diffusion coefficient of O_2 in the electrolyte (1.67×10^{-5} cm^2 s^{-1}) [29], ν is the kinematic viscosity of the electrolyte solution (1.01×10^{-2} cm^2 s^{-1}) [30], and ω is the rotation rate represented by radians per second. The average number of electrons involved in the ORR per oxygen molecule n can be determined from the slope of the linear relation between $1/j$ and $1/\omega^{1/2}$.

3. Results and discussion

3.1. Catalyst characterization

Fig. 1(a) shows a TEM image of NCNTs grown on Fe(20 wt.%)/SiO_2 at 650 °C from acetonitrile. The magnified part displays typical multi-walled bamboo-structured nanotubes obtained by iron catalysts [31]. The C–N bond length is shorter than the C–C bond, resulting in the curving of basal planes forming bamboo-like structures by nitrogen doping of the carbon nanotubes [32]. A histogram of carbon nanotube diameters, Fig. 1(b), shows that the nanotubes have an outer mean diameter of about 12.5 nm and outer diameter distribution of 5–35 nm. The dimensions of the commercial CNTs used in this work are quite similar showing an outer mean diameter of 13 nm and outer diameter distribution of 5–20 nm.

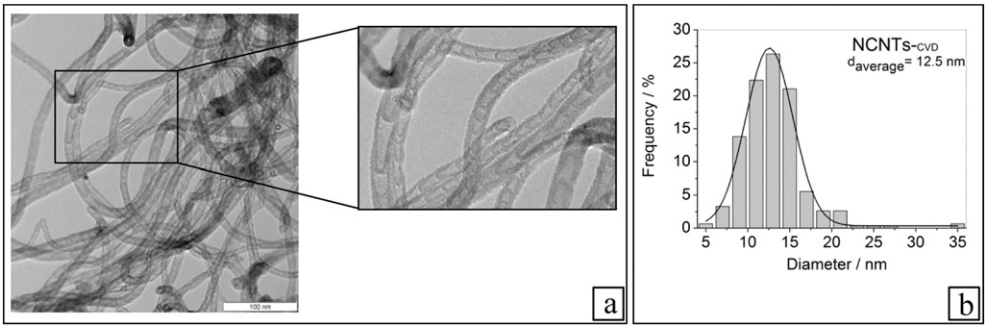

Fig. 1. (a) TEM micrograph of bamboo-structure carbon nanotubes formed by acetonitrile pyrolysis at 650 °C over Fe/SiO_2 catalyst and (b) histogram of the outer diameter distribution of carbon nanotubes.

The nitrogen loadings of nanotube samples determined by elemental analysis are summarized in Table 1.

It is seen that oxidation treatment with 5 M HNO_3 does not promote the introduction of nitrogen into the CNTs to a significant extend. The treatment with NH_3 gas led to 0.37% of nitrogen incorporated in the OCNTs. This is considerably lower than the value obtained by others [20,24], probably due to the much less severe pretreatment (5 M HNO_3 vs. HNO_3 vapor) in our work. Meanwhile, a significant amount of nitrogen (7.74%) was incorporated into the grown CNTs during the CVD process.

Raman spectroscopy was used to characterize the quality, i.e. the degree of graphitization, of the carbon nanotubes. Fig. 2 shows the Raman spectra for the samples containing nitrogen (NCNTs and $NCNTs_{-CVD}$) and two characteristic intense bands are observed for both samples. The D band, at ca. 1350 cm^{-1}, is indicative of disordered carbon, impurities and defects in CNTs. The G band, at ca. 1570 cm^{-1}, is associated with highly ordered graphite [33,34]. The intensity ratio between these bands (I_D/I_G) is normally used for the qualitative estimation of the carbon ordering degree. Generally, a lower intensity ratio indicates a higher degree of graphitization of the CNTs [35]. Fig. 2 shows the I_D/I_G ratio for both samples indicating that the nitrogen-containing carbon nanotubes sample prepared by CVD has a higher degree of ordering and probably less defects than the sample using commercial CNTs.

The Raman spectra for CNTs and OCNTs (not shown) exhibit I_D/I_G-values of 1.33 and 1.26, respectively. Obviously the incorporation of oxygen and nitrogen functional groups into the carbon nanotubes surface by HNO_3 and NH_3 treatment is less pronounced under the conditions used in this study and does only to a minor extend lead to structural defects. The same was observed by Kundu et al. [24] and it is probably due to the less severe pretreatment, as mentioned above.

Thermal gravimetric analysis (Fig. 3) indicates that no amorphous carbon, easily oxidized at around 320 °C, is present in the samples [33,36]. The mass-loss step for the NCNTs occurs at 500–700 °C which is a comparably large range of combustion. The $NCNTs_{-CVD}$ sample is oxidized at lower temperatures (450–600 °C), probably related to the higher nitrogen amount and may be due to a residual metal from the catalyst for CVD preparation. The DTG curve of $NCNTs_{-CVD}$ (see Fig. 3(b)) points to the presence of two different decomposition temperatures, one at 450–500 °C and the other at 550–600 °C, indicative of two kinds of carbon structure with distinct stability.

We thus conclude that our CNT samples mainly consist of (functionalized) CNTs while the presence of amorphous carbon, which would probably complicate the interpretation of the results, can be excluded. A lower defect density, however, was observed for the NCNTs prepared by CVD compared to the other samples.

ICP–OES measurements established platinum loadings of 7.3, 3.7, 5.8, and 4.9 wt.% for Pt/CNTs, Pt/OCNTs, Pt/NCNTs, and Pt/$NCNTs_{-CVD}$, respectively, indicating that Pt was not completely deposited onto the carbon support. This can be explained by the fact that although CNTs can anchor and disperse noble metal on the surface of CNTs, it is hard to achieve small particle size and high dispersion simultaneously [13]. Since we were aiming for small particles size, a high pH value was used in this work (pH = 10), however it has been noted that by increasing the pH of the catalyst formation solution (pH > 8.5), the metal loading is seriously reduced [37,38]. The chosen pH allowed for a good compromise between loading and particle size. Furthermore, as can be seen from the high loading of the non-functionalized CNTs, there is no clear correlation between CNT functional groups and loading, and other effects like potential of zero charge/surface charge during preparation are assumed to play a major role as well. Indeed, the lowest loading is obtained with the OCNTs, which are assumed to display the highest negative surface charge at high pH.

TEM micrographs presented in Fig. 4 visualize that the platinum nanoparticles were uniformly dispersed on the carbon support

Table 1
Carbon, hydrogen and nitrogen percentage in carbon nanotubes determined by elemental analysis.

Samples	C (%)	H (%)	N (%)
CNTs (commercial)	98.9	0.72	0.13
OCNTs	96.4	0.80	0.15
NCNTs	98.6	0.86	0.37
$NCNTs_{-CVD}$	85.3	0.71	7.74

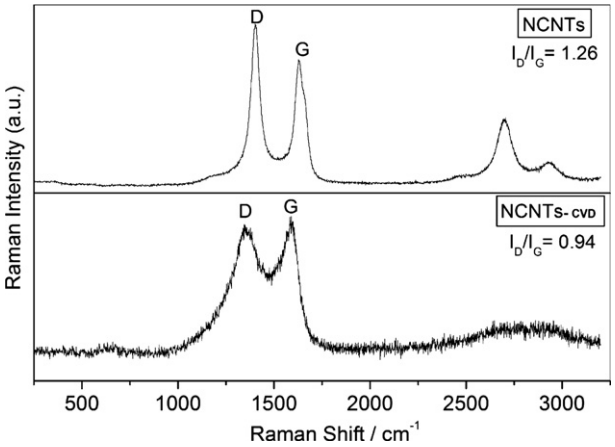

Fig. 2. Raman spectra of nitrogen-containing carbon nanotubes obtained by ammonia gas treatment (NCNTs) and CVD using acetonitrile ($NCNTs_{-CVD}$).

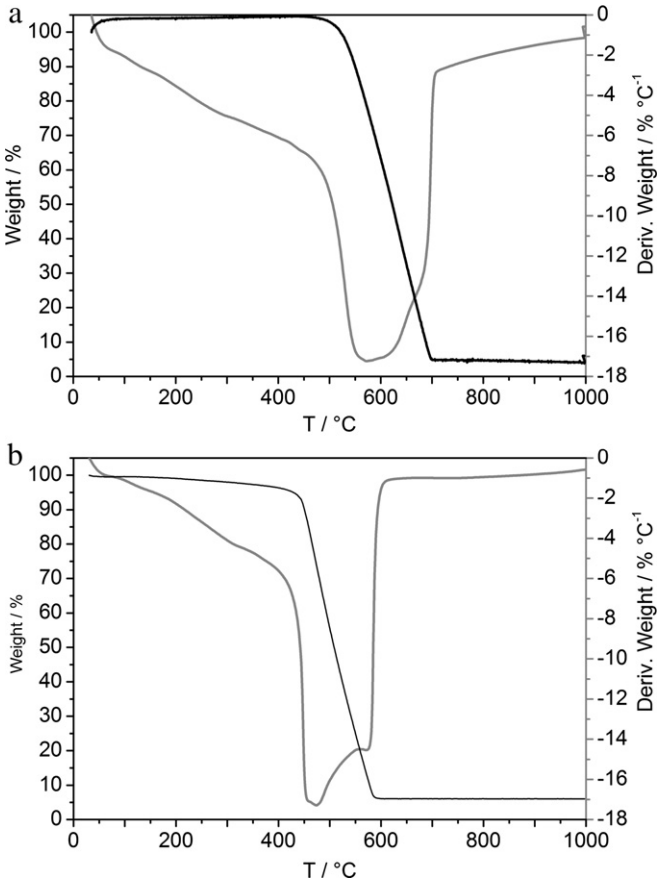

Fig. 3. TGA of nitrogen-containing carbon nanotubes obtained by (a) ammonia gas treatment (NCNTs) and (b) CVD method ($NCNTs_{-CVD}$).

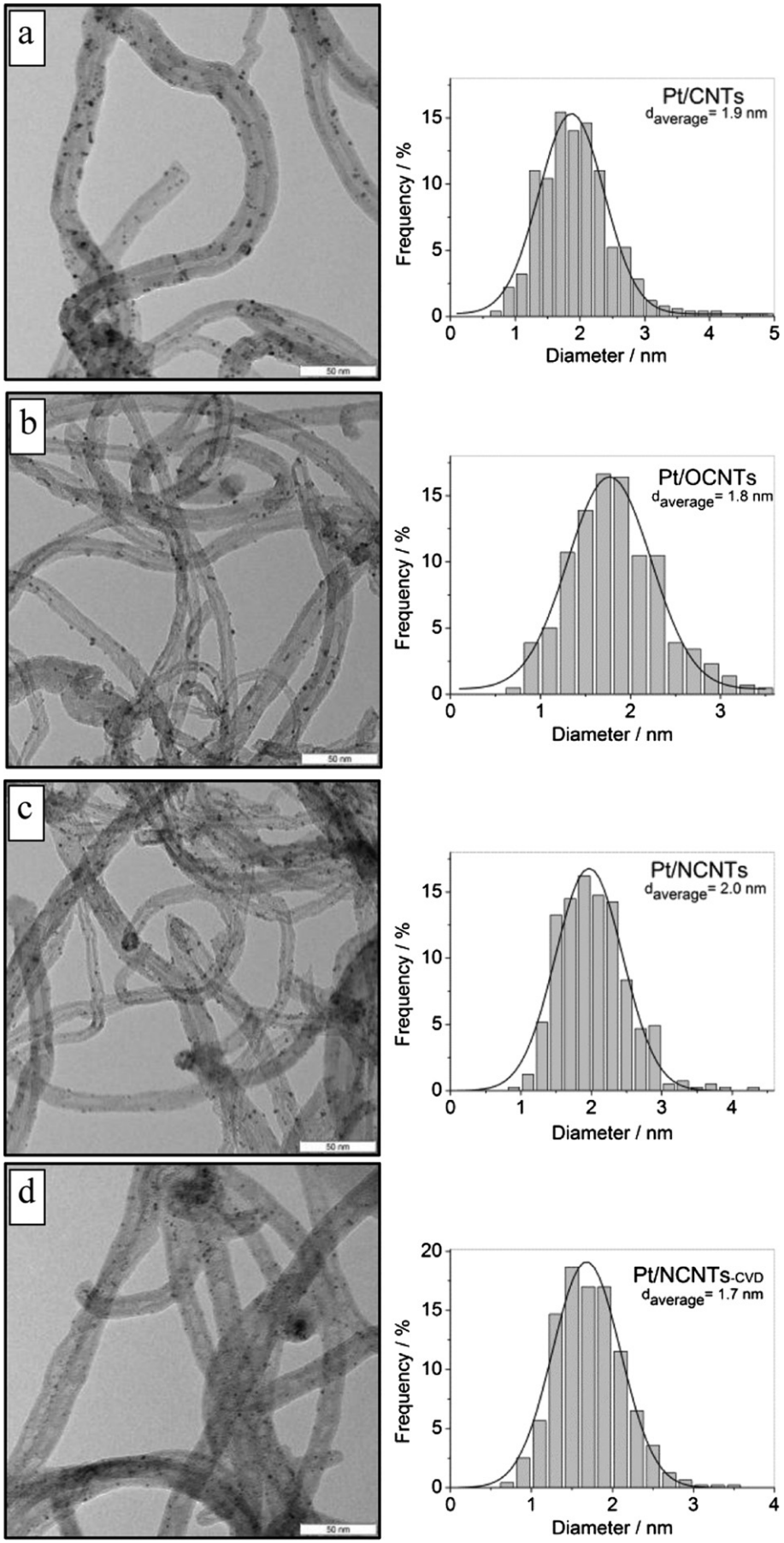

Fig. 4. TEM micrographs and corresponding histograms of particles size distribution for the different synthesized catalysts: (a) Pt/CNTs, (b) Pt/OCNTs, (c) Pt/NCNTs, and (d) Pt/NCNTs$_{-CVD}$.

with only a few agglomerations. Fig. 4 also shows the corresponding histograms, demonstrating a narrow size distribution. The Pt average diameter ($d_{average}$) of the particles is approximately 2 nm for all samples, indicating very small particles and a particle size independent of the support.

3.2. Determination of ECSA

The electrochemical surface area (ECSA) is an important property when dealing with electrocatalyst materials. It can be calculated based on the charge transfer of hydrogen adsorption/desorption (H_{upd}), or the CO oxidation charge (CO-stripping) [39–41].

The oxidation peaks of CO-stripping voltammograms, displayed in Fig. 5, were used to determine the ECSA of Pt in the working electrode based on the adsorption of CO on the platinum surface at 0.05 V. During the positive potential sweep the adsorbed CO is oxidized to carbon dioxide. The inset of Fig. 5 shows the full profile of CO-stripping voltammograms.

The electrochemical surface area for all catalysts was calculated based on Equation (2) from the charge for the CO-stripping ($Q_{CO\text{-}oxidation}$). The charge of the CO oxidation peak is calculated by integrating the stripping peak area in microcoulombs (μC). The charge required to oxidize one monolayer of CO adsorbed on a Pt surface is $Q_{CO} = 420\ \mu C\ cm^{-2}$ (equivalent to two electrons per CO molecule).

$$ECSA = Q_{CO\text{-}oxidation}/Q_{CO}L_{Pt} \quad (2)$$

L_{Pt} represents the total metal loading in the electrode (mg_{Pt}) and the ECSA is reported in $cm^2\ mg_{Pt}^{-1}$. Divided by 10, the ECSA in $m^2\ g_{Pt}^{-1}$ is obtained.

ECSAs of Pt/CNTs, Pt/OCNTs, Pt/NCNTs, and Pt/NCNTs$_{-CVD}$ catalysts were estimated by CO-stripping and found to be 102.37 $m^2\ g_{Pt}^{-1}$, 116.41 $m^2\ g_{Pt}^{-1}$, 111.62 $m^2\ g_{Pt}^{-1}$ and, 122.25 $m^2\ g_{Pt}^{-1}$, respectively. These high and similar surface area values confirm the small and similar particle sizes as observed by TEM.

Additionally, the hydrogen adsorption and desorption peaks were integrated, and the ECSA determined by the H_{upd} method was calculated by the following Equation (3):

$$ECSA = Q_{H\text{-}ads/des}/Q_H L_{Pt} = (Q_{H\text{-}ads} + Q_{H\text{-}des})/2Q_H L_{Pt} \quad (3)$$

where $Q_{H\text{-}ads/des}$ (μC) is the average of the charge for hydrogen adsorption ($Q_{H\text{-}ads}$) and desorption ($Q_{H\text{-}des}$), $Q_H = 210\ \mu C\ cm^{-2}$ is the charge required to oxidize a monolayer of hydrogen on Pt, and L_{Pt} is the total metal loading in the electrode (mg_{Pt}). Fig. 6 shows the CVs for all catalysts used to calculate the electrochemical surface area by H_{upd} charge. The ECSAs of Pt/CNTs, Pt/OCNTs, Pt/NCNTs, and Pt/NCNTs$_{-CVD}$ catalysts are indicated in Table 2, first row.

The ECSAs calculated from CO-stripping were higher than for underpotential hydrogen deposition and, because of the easier baseline correction during the integration, more reliable. The difference between ECSAs determined by these different methods was also reported by other authors [39,42,43]. Mayrhofer et al. [39] found that the surface area calculated from CO oxidation charge was about 1.4 times higher than from H_{upd}. Our study showed a ratio CO-stripping/H_{upd} between 1.33 and 1.65, in reasonable agreement with the values reported in literature. For the Pt/OCNTs catalyst a higher ratio was found (2.87) for reasons that are not clear to us at the moment.

3.3. Catalysts stability study

The main intention of this paper is to evaluate the degradation resistance of the Pt catalysts supported onto differently modified CNTs. Thus, an accelerated stress test was carried out under potential cycling conditions. In this procedure, the electrode was cycled for a total of 2500 times and the catalyst degradation was monitored at every 500 cycles by cyclic voltammetry to determinate the ECSA and polarization curves to determinate the ORR activity.

CVs were recorded from 0.05 to 1.2 V vs. RHE at a scan rate of 0.1 V s^{-1} in the absence of oxygen by purging the electrolyte solution with nitrogen at least 20 min. Fig. 7 shows the voltammetric responses before (dashed line) and after (solid line) each 500 cycles of the accelerated stress tests. Only the CVs for Pt/NCNTs$_{-CVD}$ catalyst are shown here, but all catalysts presented a similar profile.

The first CV was recorded immediately after cleaning the electrode surface (50 CV cycles, see experimental part). The hydrogen desorption peaks are less pronounced and slightly shifted to higher potentials. After the first 500 cycles, the H_{upd} peaks are developed more clearly. Probably, the initial cleaning was not sufficient to remove all adsorbed organic species remaining from the production process. However, more likely is that these changes are due to the initial structural rearrangement of the Pt catalyst (see below).

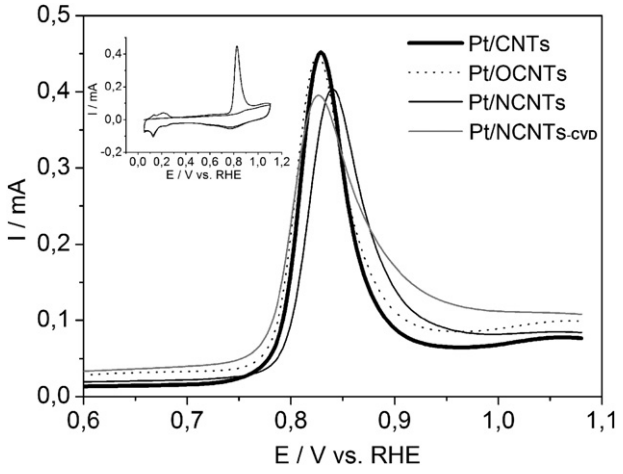

Fig. 5. Oxidation peak of CO-stripping voltammograms for all catalysts in nitrogen saturated 0.5 M H_2SO_4 electrolyte at a scan rate of 0.02 V s^{-1}. Inset showing an example of a whole CO-stripping voltammogram. Platinum loading 21 $\mu g_{Pt}\ cm^{-2}$.

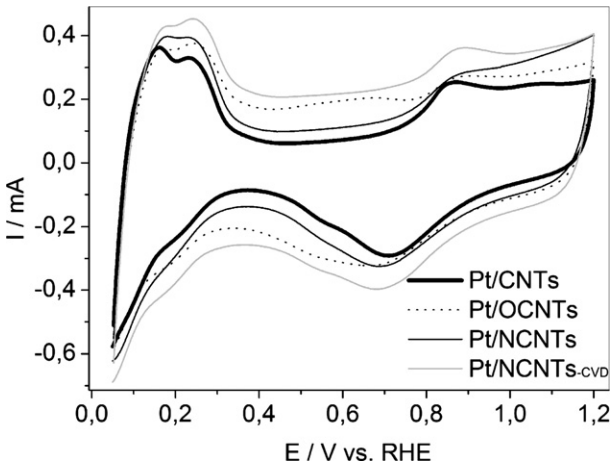

Fig. 6. Cyclic voltammograms for all catalysts in nitrogen saturated 0.1 M $HClO_4$ electrolyte at a scan rate of 0.1 V s^{-1}. Platinum loading 21 $\mu g_{Pt}\ cm^{-2}$.

Table 2
Electrochemical surface area values determined by H_{upd} after the accelerated stress tests.

Repetition	Pt/CNTs ECSA ($m^2\ g_{Pt}^{-1}$)	Pt/OCNTs ECSA ($m^2\ g_{Pt}^{-1}$)	Pt/NCNTs ECSA ($m^2\ g_{Pt}^{-1}$)	Pt/NCNTs$_{CVD}$ ECSA ($m^2\ g_{Pt}^{-1}$)
Before	61.75	40.48	83.71	81.37
1	90.17	66.25	100.58	93.76
2	88.24	68.63	99.77	91.18
3	90.18	64.76	97.31	86.81
4	88.15	62.84	87.71	86.17
5	81.59	63.59	92.94	83.59

Moreover, the peaks corresponding to platinum-oxide formation at 0.75–1.0 V and reduction at 0.7 V vs. RHE are also much better defined after the first aging procedure and the platinum oxide reduction peak is shifted toward more positive potentials. This may indicate an increase in particle size due to aging [44], however surface restructuring of Pt particles may also result in such behavior e.g. by "annealing" the surface and reducing the number of highly exposed Pt atoms. After these initial changes, the shape of the following CV profiles after each aging treatment is relatively stable indicating only minor changes in the structural composition of the catalysts.

The calculated electrochemical surface areas from H_{upd} after each accelerated stress tests are indicated in Table 2. Although, as mentioned above, CO stripping appears to be more reliable to determine ECSA, we chose to use H_{upd} due to two reasons: first of all, this approach facilitated the experimental procedure. Secondly, it is well known that CO adsorption may induce surface restructuring in Pt-based catalysts and thus may interfere with the changes introduced by aging. After the first aging step, in all cases an increase in ECSA is observed, pointing to, as discussed above, a further cleaning of the electrode surface or, more likely, to an initial restructuring: if this initial ECSA increase would be simply electrode cleaning, we would expect it to be similar for all four catalysts since they were prepared in the same way. This initial ECSA increase is less pronounced for the NCNTs-supported catalysts, pointing to a better stabilization of the Pt nanoparticles on these supports. Afterward, a small and non-linear decay of ECSA can be observed, probably pointing to a slight increase in particle size. Other mechanisms discussed to explain reduced ECSA are detachment of whole particles [45].

It is important to note that the loss in ECSA on the CNT-supported samples in this study is much less pronounced than in aging studies in the literature on carbon black-supported Pt catalysts using a different aging protocol [45] as well as on Pt/C investigated by us under exactly the same conditions as the Pt/CNT samples (see Supporting information S1). This is a clear indication that CNTs may provide better stability when used as electrocatalyst support in applications like e.g. fuel cells.

Considering Table 2, the comparably minor differences in the development of ECSA between the different Pt/CNT samples are striking. It is typically assumed that CNT functionalization should stabilize the deposited Pt particles due to interaction with surface functional groups. Since the presence of amorphous material or influences of other structural features like diameter can be excluded in our study, obviously the interaction with the surface graphene sheets of the CNTs is already sufficient to establish such a stabilizing effect. Given the fact that the highest catalyst loading was also obtained with the non functionalized CNTs, the necessity of surface functionalization should be reconsidered in light of the individual catalyst preparation route. While it may be necessary to functionalize CNTs for high loading catalysts prepared by impregnation or other techniques, our results point to the fact that the situation changes for low loading catalysts prepared by the polyol technique.

Besides ECSA, the development of the Pt mass and surface-specific activities induced by the accelerated stress test is of high interest. RDE experiments were performed from 0.05 V to 1.05 V vs. RHE at a scan rate of 0.005 V s^{-1} at 400, 900, and 1600 rpm. Fig. 8 compares the curves, of all synthesized catalysts, obtained at 900 rpm, after the second stress test repetition, additional results of a Koutecky–Levich analysis can be found in the supporting information (Figure S2).

The typical behavior with three different regions: kinetically controlled region, mixed kinetically and diffusion controlled region, and diffusion-controlled region can be observed. Slight differences in the diffusion-limited currents between the catalysts are observed, which were reproducible (i.e., do not depend on the quality of the individual electrode). The differences in diffusion limited currents point to a slightly different average number of electrons transferred per oxygen molecule. The respective values calculated from the Koutecky–Levich-Plot (Figure S2 in supporting information) for Pt/CNTs, Pt/OCNTs, and Pt/NCNTs were 3.71, 3.69, and 3.68, respectively, while Pt/NCNTs$_{CVD}$ yielded 4.11 electrons.

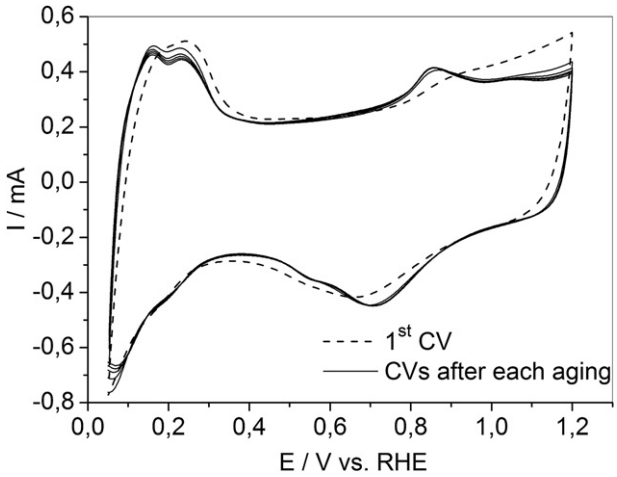

Fig. 7. CVs of catalyst Pt/NCNTs$_{CVD}$ before the accelerated stress tests (---) and after each aging test (—). The aging treatment consisted in 5 repetitions of 500 cycles each, between 0.1 and 1.3 V vs. RHE at a scan rate of 1 V s^{-1}, in N_2 saturated 0.1 M $HClO_4$.

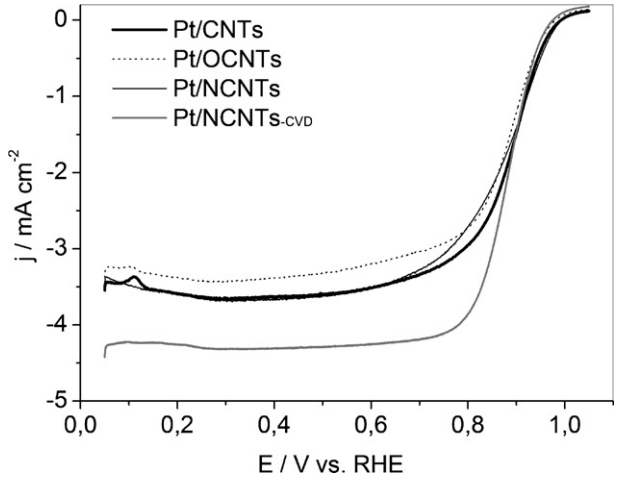

Fig. 8. ORR polarization curves in oxygen-saturated 0.1 M $HClO_4$ at 900 rpm on different synthesized catalysts: (—) Pt/CNTs, (···) Pt/OCNTs, (·-·) Pt/NCNTs, and (—) Pt/NCNTs$_{CVD}$. Scan rate: 0.005 V s^{-1}.

Although this is higher than the maximum theoretical value of 4 (i.e., there is a certain error in this method), it might indicate that Pt/NCNTs$_{CVD}$ produces less H_2O_2. The reasons for this difference are not clear to us at the moment and might include H_2O_2 reduction at the CNTs themselves. The half-wave potentials ($E_{1/2}$) are practically the same in all catalysts, except Pt/OCNTs that presented $E_{1/2}$ slightly more negative. The Koutecky–Levich (Equation (1)) was used to analyze the ORR kinetics. The kinetic current density (j_{kin}) at $E = 0.90$ V vs. RHE was calculated and the Pt surface-specific activities are summarized in Table 3. The surface-specific activity of the catalysts was determined by dividing the observed kinetic current (mA/electrode) at 0.9 V by the Pt ECSA (cm^2_{Pt}/electrode).

While it is admittedly difficult to quantitatively compare the individual catalysts due to a certain uncertainty in the determination of ECSA, qualitatively clear differences in the development of surface-specific activity with aging can be observed. While CNTs and OCNTs supported samples show an initial clear drop in surface-specific activity during the first one or two stress test cycles and then exhibit a slight increase in surface-specific activity, this initial drop is not observed with the NCNTs supported ones, where the surface-specific activity remains constant or increases right from the beginning. Furthermore it is obvious that for the CNTs and OCNTs samples, the ECSA increase in the first one or two cycles is inversely proportional to the surface-specific activity, which is equivalent to the statement that the overall activity (i.e., the intrinsic activity of a given amount of catalyst) is constant. A simple cleaning effect would not result in such behavior but the surface-specific activity should remain constant. Thus, these findings corroborate the view that the measured ECSA increases with concurrent decrease in surface-specific activity results from initial restructuring effects, i.e. an initially preferential structure for ORR rearranges to a less favorable one.

Furthermore it is well known that the ORR at Pt is a structure sensitive reaction with larger particles exhibiting a higher surface specific activity. An increase in specific activity observed for nearly all samples after the initial rearrangement thus may point to slow particle growth, in agreement with the slight loss in ECSA occurring concurrently.

On the other hand, a (less pronounced) increase in ECSA for the NCNTs supported catalysts while the surface specific activity remains constant points to an increase in the overall activity (i.e., the intrinsic activity of a given amount of catalyst). Although the exact reason cannot be deduced from our results, it is clear that Pt catalysts supported on NCNTs behave differently during the accelerated stress test and are more stable than OCNTs and CNTs supported samples with respect to surface-specific activity. Tentatively this behavior is attributed to a stronger interaction of the basic NCNTs with the Pt, leading to a stabilization of the Pt particles. In this regard, it is interesting to note that the surface-specific activity of the Pt/C catalyst with carbon black as support shows an increase in surface-specific activity with values of 0.209, 0.225, 0.257, 0.313, 0.384 and 0.463 mA cm^{-2}_{Pt} before and after subsequent stress tests. However, this increase is overcompensated by a drastic loss in surface area (Fig. S1) leading to a strong loss in intrinsic catalyst activity.

Table 3
Pt surface-specific activities of oxygen reduction on CNTs catalysts in each repetition. $E = 0.9$ V vs. RHE.

Repetition	Pt surface-specific activities (mA cm^{-2}_{Pt})			
	Pt/CNTs	Pt/OCNTs	Pt/NCNTs	Pt/NCNTs$_{CVD}$
Before	0.186	0.220	0.113	0.150
1	0.120	0.141	0.105	0.154
2	0.129	0.125	0.108	0.172
3	0.131	0.135	0.093	0.188
4	0.134	0.147	0.093	0.179
5	0.145	0.146	0.101	0.200

4. Conclusions

Four different functionalized carbon nanotubes supported Pt nanoparticles (2 nm) catalysts were prepared and investigated. Carbon nanotubes containing 7.74% of nitrogen were synthesized by chemical vapor deposition using acetonitrile as carbon and nitrogen source. TEM images showed typical multi-walled bamboo-structures nanotubes with a uniform outer mean diameter of about 12.5 nm. Raman spectroscopy indicated that NCNTs$_{CVD}$ showed higher carbon ordering degree than the sample using commercial carbon nanotubes. All electrocatalysts presented a high surface area confirming the small particle size observed by TEM. Catalyst resistance to degradation was evaluated through an accelerated stress test where the degradation was monitored, every 500 cycles, by ECSA loss and ORR activity. Although some changes were observed in the hydrogen desorption peaks after the first 500 cycles, the following CVs were relatively stable after each aging treatment with only a small and non-linear decay, probably due to a slight increase in particle size and detachment of whole particles. Strikingly the stability of the Pt catalysts during electrochemical treatment is not influenced by the presence of functional groups, and the stability of all CNT supported samples is much higher than with carbon black-supported ones. Furthermore, the catalyst loading achieved with the polyol technique was highest for the non-functionalized CNTs. With respect to surface-specific activity, Pt catalysts supported on NCNTs are more stable than OCNTs and CNTs supported samples.

Acknowledgments

Dr. Daniela Mezalira acknowledges the National Council for Scientific and Technological Development (CNPq), Brazil, for a postdoctoral scholarship. The Inderdisciplinary Centre of Materials Science and the Institute of Physics – Allgemeine Werkstoffwissenschaften – of the Martin-Luther-Universität Halle-Wittenberg are gratefully acknowledged for providing access to TEM facilities. The central facilities of the Department of Chemistry and the Department of Geology of Martin-Luther-Universität helped with elemental analysis and ICP–OES. Parts of this work were supported by grants DFG INST 271/285-1 and DFG INST 271/286-1 of the German research foundation.

Appendix A. Supplementary material

Supplementary material associated with this article can be found, in the online version, at http://dx.doi.org/10.1016/j.jpowsour.2012.12.025.

References

[1] X.-Z. Yuan, H. Wang, in: J. Zhang (Ed.), PEM Fuel Cell Electrocatalysts and Catalyst Layers: Fundamentals and Applications, Springer, London, 2008, pp. 1–85.
[2] H.A. Gasteiger, S.S. Kocha, B. Sompalli, F.T. Wagner, Appl. Catal. B 56 (2005) 9–35.
[3] A.A. Gewirth, M.S. Thorum, Inorg. Chem. 49 (2010) 3557–3566.
[4] S. Schimpf, M. Bron, in: D. Stolten, B. Emonts (Eds.), Fuel Cell Science and Engineering: Materials, Processes, Systems and Technology, Wiley VCH, Weinheim, 2012, pp. 407–438.
[5] K.P. De Jong, Curr. Opin. Solid State Mater. Sci. 4 (1999) 55–62.
[6] R. Borup, J. Meyers, B. Pivovar, Y.S. Kim, R. Mukundan, N. Garland, D. Myers, M. Wilson, F. Garzon, D. Wood, P. Zelenay, K. More, K. Stroh, T. Zawodzinski, J. Boncella, J.E. McGrath, O.M. Inaba, K. Miyatake, M. Hori, K. Ota, Z. Ogumi,

S. Miyata, A. Nishikata, Z. Siroma, Y. Uchimoto, K. Yasuda, K.-i. Kimijima, N. Iwashita, Chem. Rev. 107 (2007) 3904–3951.
[7] K. Wikander, H. Ekström, A.E.C. Palmqvist, G. Lindbergh, Electrochim. Acta 52 (2007) 6848–6855.
[8] M.S. Wilson, F.H. Garzon, K.E. Sickafus, S. Gottesfeld, J. Electrochem. Soc. 140 (1993) 2872–2877.
[9] P.J. Ferreira, G.J. La O', Y. Shao-Horn, D. Morgan, R. Makharia, S. Kocha, H.A. Gasteiger, J. Electrochem. Soc. 152 (2005) A2256–A2271.
[10] R.M. Darling, J.P. Meyers, J. Electrochem. Soc. 150 (2003) A1523–A1527.
[11] K. Yasuda, A. Taniguchi, T. Akita, T. Ioroi, Z. Siroma, Phys. Chem. Chem. Phys. 8 (2006) 746–752.
[12] K.J.J. Mayrhofer, J.C. Meier, S.J. Ashton, G.K.H. Wiberg, F. Kraus, M. Hanzlik, M. Arenz, Electrochem. Commun. 10 (2008) 1144–1147.
[13] B. Wu, Y. Kuang, X. Zhang, J. Chen, Nano Today 6 (2011) 75–90.
[14] Y. Shao, J. Liu, Y. Wang, Y. Lin, J. Mater. Chem. 19 (2009) 46–59.
[15] D. Sebastián, A.G. Ruíz, I. Suelves, R. Moliner, M.J. Lázaro, V. Baglio, A. Stassi, A.S. Aricò, Appl. Catal. B 115–116 (2012) 269–275.
[16] F. Hasché, M. Oezaslana, P. Strasser, Phys. Chem. Chem. Phys. 12 (2010) 15251–15258.
[17] S.-H. Liu, M.-T. Wu, Y.-H. Lai, C.-C. Chiang, N. Yu, S.-B. Liu, J. Mater. Chem. 21 (2011) 12489–12496.
[18] V.V. Strelko, V.S. Kuts, P.A. Thrower, Carbon 38 (2000) 1499–1503.
[19] G. Wu, D. Li, C. Dai, D. Wang, N. Li, Langmuir 24 (2008) 3566–3575.
[20] T.C. Nagaiah, S. Kundu, M. Bron, M. Muhler, W. Schuhmann, Electrochem. Commun. 12 (2010) 338–341.
[21] N. Alexeyeva, E. Shulga, V. Kisand, I. Kink, K. Tammeveski, J. Electroanal. Chem. 648 (2010) 169–175.
[22] N.G. Sahoo, S. Rana, J.W. Cho, L. Li, S.H. Chan, Prog. Polym. Sci. 35 (2010) 837–867.
[23] S. Kundu, Y. Wang, W. Xia, M. Muhler, J. Phys. Chem. C 112 (2008) 16869–16878.
[24] S. Kundu, W. Xia, W. Busser, M. Becker, D.A. Schmidt, M. Havenith, M. Muhler, Phys. Chem. Chem. Phys. 12 (2010) 4351–4359.
[25] S. Van Dommele, K.P. De Jong, A. Romero-Izquirdo, J.H. Bitter, in: E.M. Gaigneaux, M. Devillers, D.E. De Vos, S. Hermans, P.A. Jacobs, J.A. Martens, P. Ruiz (Eds.), Studies in Surface Science and Catalysis, vol. 162, 2006, pp. 29–36.
[26] W.X. Chen, J.Y. Lee, Z. Liu, Chem. Commun. 21 (2002) 2588–2589.
[27] S.-B. Yin, L. Luo, S.-Y. Jing, Q.-Q. Zhu, Y.-H. Qiang, Acta Phys. Chim. Sin. 28 (2012) 85–89.
[28] W. Yu, W. Tu, H. Liu, Langmuir 15 (1998) 6–9.
[29] C. Song, J. Zhang, in: J. Zhang (Ed.), PEM Fuel Cell Electrocatalysts and Catalyst Layers: Fundamentals and Applications, Springer, London, 2008, pp. 89–134.
[30] N.M. Marković, H.A. Gasteiger, B.N. Grgur, P.N. Ross, J. Electroanal. Chem. 467 (1999) 157–163.
[31] W.Y. Wong, W.R.W. Daud, A.B. Mohamad, A.A.H. Kadhum, E.H. Majlan, K.S. Loh, Diamond Relat. Mater. 22 (2012) 12–22.
[32] X. Li, J. Liu, Y. Zhang, Y. Li, H. Liu, X. Meng, J. Yang, D. Geng, D. Wang, R. Li, X. Sun, J. Power Sources 197 (2012) 238–245.
[33] W. Li, H. Wang, Z. Ren, G. Wang, J. Bai, Appl. Catal. B 84 (2008) 433–439.
[34] T. Belin, F. Epron, Mater. Sci. Eng. B 119 (2005) 105–118.
[35] Q. Zhao, Y. Li, X. Zhou, T. Jiang, C. Li, H. Yin, Superlatt. Microstruct. 47 (2010) 432–441.
[36] D.Z. Mezalira, L.D. Probst, S. Pronier, Y. Batonneau, C. Batiot-Dupeyrat, J. Mol. Catal. A: Chem. 340 (2011) 15–23.
[37] H.-S. Oh, J.-G. Oh, Y.-G. Hong, H. Kim, Electrochim. Acta 52 (2007) 7278–7285.
[38] L. Ren, Y. Xing, Electrochim. Acta 53 (2008) 5563–5568.
[39] K.J.J. Mayrhofer, D. Strmcnik, B.B. Blizanac, V. Stamenkovic, M. Arenz, N.M. Markovic, Electrochim. Acta 53 (2008) 3181–3188.
[40] R. Chetty, S. Kundu, W. Xia, M. Bron, W. Schuhmann, V. Chirila, W. Brandl, T. Reinecke, M. Muhler, Electrochim. Acta 54 (2009) 4208–4215.
[41] D.C. Higgins, D. Meza, Z. Chen, J. Phys. Chem. C 114 (2010) 21982–21988.
[42] O.A. Baturina, B.D. Gould, Y. Garsany, K.E. Swider-Lyons, Electrochim. Acta 55 (2010) 6676–6686.
[43] C. Wang, M. Chi, D. Li, D. Strmcnik, D. Van Der Vliet, G. Wang, V. Komanicky, K.-C. Chang, A.P. Paulikas, D. Tripkovic, J. Pearson, K.L. More, N.M. Markovic, V.R. Stamenkovic, J. Am. Chem. Soc. 133 (2011) 14396–14403.
[44] K. Jayasayee, J.A.R.V. Veen, T.G. Manivasagam, S. Celebi, E.J.M. Hensen, F.A. De Bruijn, Appl. Catal. B 111–112 (2012) 515–526.
[45] K. Hartl, M. Hanzlik, M. Arenz, Energy Environ. Sci. 4 (2011) 234–238.